Intensity detecting refractive index sensors with long-period fiber gratings written in STS structure

Zuliang Ruan (阮祖亮)[1,2], Li Pei (裴 丽)[1,2,*], Jingjing Zheng (郑晶晶)[1,2], Jianshuai Wang (王建帅)[1,2], Liangying Wu (吴良英)[1,2], Tigang Ning (宁提纲)[1,2], and Ji Wang (王 吉)[1,2]

[1]*Institute of Lightwave Technology, Beijing Jiaotong University, Beijing 100044, China*
[2]*Key Laboratory of All Optical Network and Advanced Telecommunication Network of Ministry of Education, Beijing Jiaotong University, Beijing 100044, China*
**Corresponding author: lipei@bjtu.edu.cn*

Received January 4, 2019; accepted March 22, 2019; posted online June 10, 2019

A refractive index intensity detecting sensor with long-period grating written in the single-mode–thin-core–single-mode fiber (STS) structure is proposed and optimized theoretically. The sensor is composed of two single-mode fibers connected by a section of long-period fiber grating fabricated on thin-core fiber. After optimization and benefitting from the phase matching point, the loss peak of the structure can reach 62.8 dB theoretically. The wavelength of the characteristic peak is fixed at the phase matching point, so intensity detection can be achieved. The sensitivity can reach 272.5 dB/RIU. The structural optimization in this Letter provides a reference for the fabrication of an easy-made all-fiber sensor without extra cladding.

OCIS codes: 060.2370, 060.2300.
doi: 10.3788/COL201917.070601.

All-fiber refractive index (RI) sensors are widely expected in fields such as industry, civil engineering, biomedicine, chemistry, aerospace, and petroleum because of their superior anti-electromagnetic interference and high sensitivity. Sensors based on a Mach–Zehnder interferometer (MZI)[1,2], fiber Bragg gratings (FBGs)[2–4], and long-period fiber gratings (LPFGs)[5–9] have received extensive attention and research. Among them, the single-mode–thin-core–single mode fiber (STS)[10,11] structure, which is composed of MZI sensors, has the merits of being simple[1], easy to implement, adjustable, and multi-feature sensing. Currently, the RI detection methods based on the STS structure are mainly using FBGs[2], LPFG cascades[6], and MZI-structured sensors[1,2,11]. Through the detection of wavelength drift, RI sensing can be achieved. These solutions are achieved by etching the cladding to increase the effect of the external RI on the effective RI, or by increasing the energy of the cladding mode by the effect of LPFG or tilted FBG (TFBG)[12–14]. By coating a high RI material outside the cladding, the sensitivity of the RI can be significantly increased[15]. Due to the small core structure of the thin-core fiber (TCF), the STS structure can stimulate a series of cladding modes in the connected area[10,16]. When the TCF cladding is etched, a portion of the external RI material acts as a waveguide structure, and high-sensitivity measurements of environmental parameters can be performed. Compared with a single-mode–multi-mode–single-mode fiber (SMS)[17] and single-mode–few-mode–single-mode fiber (SFS)[18], STS has the basic mode of occupying an absolute advantage. The first few modes were stimulated by SMS and SFS, and the energy was relatively uniform, so the impact of other modes on MZI could not be ignored.

In this Letter, we increase the excitation of the cladding mode by directly writing LPFG on the TCF to achieve a comb spectrum with an increased extinction ratio (ER). We theoretically discuss the possibility and conditions of improving the overall performance by optimizing the MZI with an LPFG and analyze the characteristics of the comb filter of this structure. The step fiber as the simplest structure can make the structure more stable and simple. The structure improves sensor repeatability and reliability through axial alignment. Due to the strong fundamental mode, the energy of the unexcited modes is extremely low and can be ignored. In this way, the best power balance of the two coupled modes can be obtained through calculation. Based on these, the sensor with light intensity detection for external RI sensing is proposed. The structure has two advantages that are easy to implement and use.

The structure of the proposed sensor, which consists of two single-mode fibers (SMFs) and a section of TCF, is shown in Fig. 1. The length of the LPFG in the TCF is 100 mm, the total length of the TCF is 400 mm, and the entire axis is aligned with no eccentricity. The power

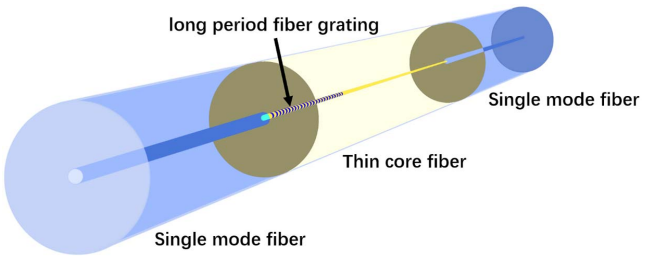

Fig. 1. Structure of the sensor.

is coupled into the TCF via the SMF excitation on the first junction. Because of the axial alignment, only the circular-symmetric linearly polarized (LP_{0n}) mode is excited. Part of the LP_{01} mode power is coupled to LP_{02} through the LPFG and then propagates independently through the following segment to interfere at the second end face to form a comb spectrum.

In order to analyze the transmission spectrum of the structure, it is divided into four substructures to be analyzed. The first is to analyze the coupling of the SMF to the TCF. In the SMF, there is only fundamental mode transmission. Because this structure is an exact axis alignment structure, it can be simplified as the coupling of the LP_{01} mode of the SMF and the LP_{0n} mode of the TCF. The coupling coefficient of the junction can be expressed as follows[17,19]:

$$\eta_n = \frac{\left[\int_0^{2\pi}\int_0^{\infty}\psi_s(r,\varphi)\psi_{0n}^*(r,\varphi)r\mathrm{d}r\mathrm{d}\varphi\right]^2}{\int_0^{2\pi}\int_0^{\infty}|\psi_s(r,\varphi)|^2 r\mathrm{d}r\mathrm{d}\varphi\int_0^{2\pi}\int_0^{\infty}|\psi_{0n}(r,\varphi)|^2 r\mathrm{d}r\mathrm{d}\varphi}, \tag{1}$$

where ψ_s is the fundamental mode distribution of the SMF, and ψ_{0n} is the LP_{0n} mode distribution of the TCF. In a circle-symmetrical step-index fiber, the LP_{0n} mode can be described with the following Bessel function[10]:

$$\psi_{0n}(r,\varphi) = \begin{cases} a_i J_0\left(\frac{U_i r}{a}\right) + b_i N_0\left(\frac{U_i r}{a}\right) & kn_i \geq \beta \\ a_i I_0\left(\frac{U_i r}{a}\right) + b_i K_0\left(\frac{U_i r}{a}\right) & kn_i < \beta \end{cases}, \tag{2}$$

where $U_i^2 = |(k^2 n_i^2 - \beta^2)|a^2$, with $k = \frac{2\pi}{\lambda}$, represents the normalized transverse propagation constant of the layer, β is the propagation constant, and b_1 and a_3 are coefficients, which are zero.

The transmission matrix of an LPFG of length L_1 can be described as

$$\begin{aligned} F_1 &= \begin{pmatrix} t & r \\ r & t^* \end{pmatrix} \\ &= \begin{pmatrix} \cos(\gamma L_1) + i\frac{\sigma}{\gamma}\sin(\gamma L_1) & i\frac{k_n}{\gamma}\sin(\gamma L_1) \\ i\frac{k_n}{\gamma}\sin(\gamma L_1) & \cos(\gamma L_1) - i\frac{\sigma}{\gamma}\sin(\gamma L_1) \end{pmatrix}. \end{aligned} \tag{3}$$

In the formula, $\gamma = \sqrt{\sigma^2 + k_n^2}$, $\sigma = \delta + \frac{\sigma_1 - \sigma_n}{2} - \frac{1}{2}\frac{\mathrm{d}\phi}{\mathrm{d}z}$, $\delta = \left(\frac{\beta_1 - \beta_n}{2}\right) - \frac{\pi}{\Lambda}$, k_n is the linear coupling coefficient of the LP_{01} and LP_{0n} modes respectively, and σ_1, σ_n are self-coupling coefficients of LP_{01} and LP_{0n}, respectively.

At the end of a TCF of length z, its field distribution can be described by the following equation without considering the addition of LPFG[18]:

$$E_{\mathrm{tcf}} = \sum_{n=1}^{N}\sqrt{\eta_n}\psi_{0n}(r,\varphi)\exp(j\beta_n z), \tag{4}$$

where β_n is the propagation constant of the LP_{0n} mode, and N is the total number of modes in the TCF. For the comb filter, which considers only the grating-coupled LP_{01} and LP_{0n} modes, the overall transfer function can be expressed as

$$T_{\mathrm{total}} = |F_0(L_0)\cdot F_1\cdot F_0(L_2)|^2. \tag{5}$$

Here, $F_0(L)$ is the transmission matrix of the TCF, where the coupling structure is the same on both sides by default, and the coupling coefficient is exactly the same:

$$F_0(L) = \begin{pmatrix} \sqrt{\eta_1}\exp(j\beta_1 L) & 0 \\ 0 & \sqrt{\eta_n}\exp(j\beta_n L) \end{pmatrix}. \tag{6}$$

In the case of a dense comb spectrum, it can be approximately seen that the coupling coefficient k of the grating between the two peaks is similar, so the ER can be expressed as

$$\mathrm{ER} = 10\lg\left(\frac{T_{\max}}{T_{\min}}\right) = 20\lg\left|\frac{(t+r)\eta_1 + (r+t^*)\eta_n}{(t-r)\eta_1 + (r-t^*)\eta_n}\right|. \tag{7}$$

Taking into account the coupling loss (in dB), it can be approximately simplified as

$$\mathrm{Loss} = -20\lg(\eta_1 + \eta_n). \tag{8}$$

From previous analysis, it can be known that for an STS structure with LPFG, the ER of the comb spectrum depends not only on the coupling efficiency of LP_{01} and LP_{0n}, but also on the coupling coefficient of LPFG. The coupling coefficients of various modes at different core radii are firstly analyzed and then shown in Table 1. Consider that the selected TCF cladding radius is $a_{t,2} = 52.5$ μm, the core RI is $n_{t,\mathrm{co}} = 1.4438$, the cladding RI is $n_{t,\mathrm{cl}} = 1.4378$, the RI of the SMF is consistent with TCF, the core radius of the SMF is $a_{s,2} = 4$ μm, and the cladding radius of the SMF is $a_{s,2} = 62.5$ μm at operating wavelength of $\lambda = 1550$ nm.

From Table 1, it is easy to find that η_1, which dominates the LP_{01} mode, increases rapidly as the core radius increases, while the other modes decrease rapidly. When the core radius reaches 1.5 μm, the mode coupling coefficients after LP_{05} are less than 0.05. The effect on the

Table 1. Coupling Coefficients of Modes at Different Core Radii

η	$a_{t,1} = 1.3$ μm	$a_{t,1} = 1.5$ μm	$a_{t,1} = 1.7$ μm
LP_{01}	0.2420	0.4003	0.6020
LP_{02}	0.2024	0.1645	0.0906
LP_{03}	0.1787	0.1469	0.0997
LP_{04}	0.1376	0.1096	0.0763
LP_{05}	0.0957	0.0735	0.0505
LP_{06}	0.0616	0.0454	0.0303

transmission spectrum can be ignored. In the case of thin core, the sum of the LP_{01} and LP_{02} modes is the largest. The LP_{01} coupling coefficient is above 0.5 and dominates over the other modes when the core is thick. Therefore, only the coupling between the LP_{01} and LP_{02} modes is considered here.

In order to more accurately analyze the transmission spectrum and because of the wide bandwidth of the LPFG, we also analyzed the relationship between the coupling coefficient and the wavelengths, and the results are shown in Fig. 2. As η_1 decreases with increasing wavelength, and other modes increase, LP_{02} mode has $\eta_2 < \eta_3$ at short wavelengths, but as the wavelength increases, the growth rate is faster, and $\eta_2 > \eta_3$ at long wavelengths.

The reason why η_2 is so weak is that in the TCFs cores that are too small can only support the LP_{01} mode, while other modes belong to the cladding modes, so most of the power distribution is concentrated in the core.

After considering the influence of LPFG, according to the Eqs. (3) and (5), the enveloping curve of the overall comb spectrum is the loss of the LPFG, as shown in Fig. 3(b). When α is large, this equation degenerates into the loss spectrum of an LPFG, and the maximum ER can reach 62.8 dB. The external RI in Fig. 3 is set to one.

In Fig. 3(a), the effect of different periods on the transmission spectrum can be seen. Among them, the overall dips will change to longer wavelengths as the period

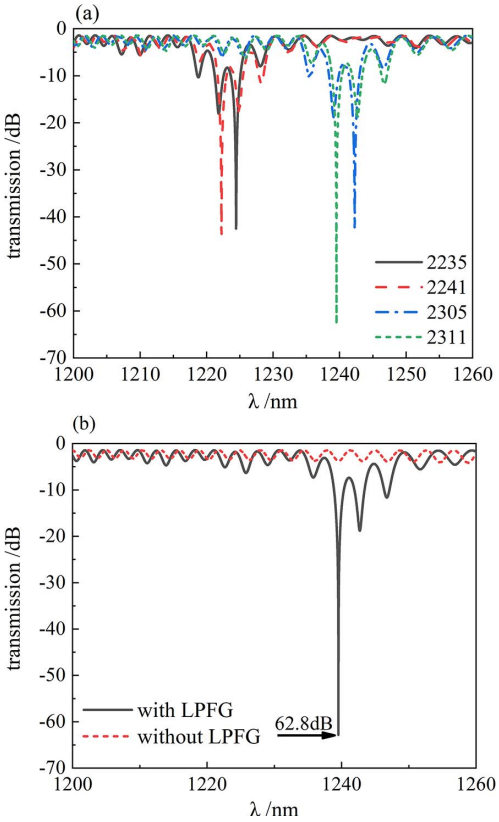

Fig. 3. (a) Transmission spectrum of LPFGs with different periods. (b) Maximum ER after adding LPFGs.

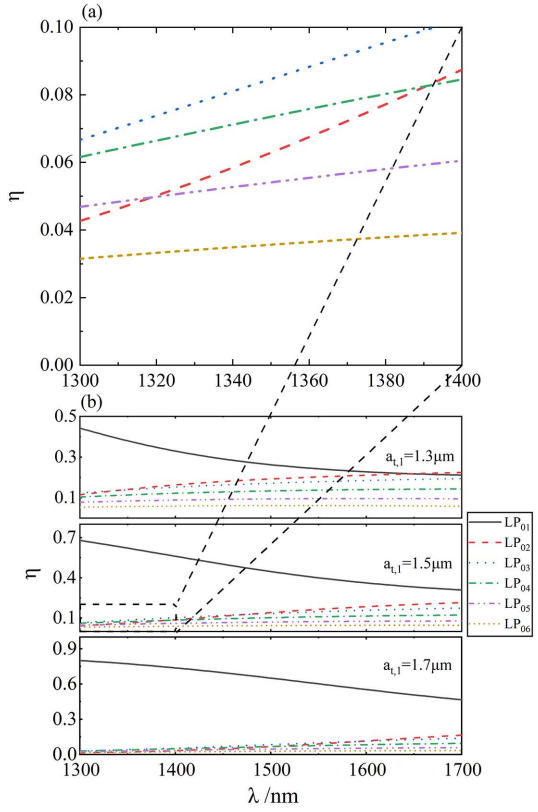

Fig. 2. (a) Coupling coefficient curve in the range of the dotted line in (b). (b) The curve of the coupling coefficient as a function of wavelength from 1300 to 1700 nm.

increases and the periodicity changes over a larger range, and, at the same time, ER will also rise. However, unlike the long-period grating transmission spectrum in the SMF, the effect of LPFG on the comb spectrum is at the right side first and then the left side.

Consider the parameters of the TCF, $a_{t,1} = 1.6$ μm, $a_{t,2} = 27.5$ μm, $n_{t,\mathrm{co}} = 1.4438$, and $n_{t,\mathrm{cl}} = 1.4378$. The results are shown in Figs. 4 and 5. Different from the SMF with LPFG, there are two dips in the structure at both sides of the phase matching point. In this structure, the effective RI difference of the LP_{01} and LP_{02} modes exhibits a parabolic distribution as the wavelength changes.

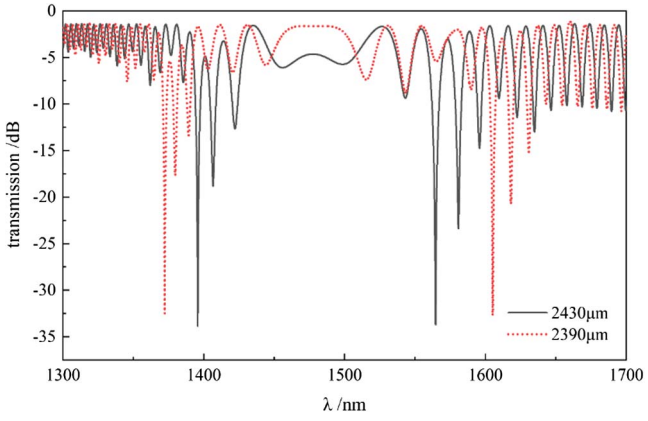

Fig. 4. Double-sided dips at different grating periods.

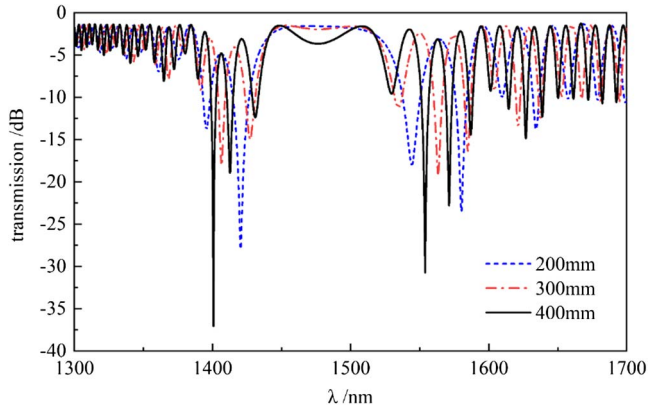

Fig. 5. Transmission of TCF with different lengths.

This phenomenon is reflected in Fig. 4 as the phase matching point[20]. As the period of the LPFG becomes longer, the dip at the short wavelength shifts toward the long wavelength, and the amplitude decreases, but the dip at the long wavelength shifts toward the short wavelength, and the amplitude increases. In Fig. 5, as the length of the TCF increases, the density of the comb spectrum increases.

In order to find the higher modes' influence on the transmission, Fig. 6 shows the transmission spectrum of the first four modes after low-pass filtering and the transmission spectrum of the first two modes. It can be seen that after filtering, there is only a wavelength shift near the phase matching point. The grating period is 3400 μm.

After the above analysis, under this structure, as the wavelength increases, the difference of the coupling coefficient will gradually decrease, making the comb spectrum more obvious and the ER significantly improve, but the overall loss also increases.

When the grating period just matches the phase matching point, the wavelength shifts when the change of the external RI is fixed there, and only the light intensity changes. By specially designing the center wavelength of the grating, intensity detection for the change of the outside RI can be realized. Considering the parameters of the TCF, $a_{t,1} = 1.6$ μm, $a_{t,2} = 27.5$ μm, $n_{t,\mathrm{co}} = 1.4438$, $n_{t,\mathrm{cl}} = 1.4378$, the grating period is 2475 μm, the length of the LPFG is set to 100 mm, and the simulation results are shown in Fig. 7. Since the intensity detection does not require complicated and expensive spectrometers, the solution has a broader application space. The transmission spectrum changes with the external RI, as shown in Fig. 7.

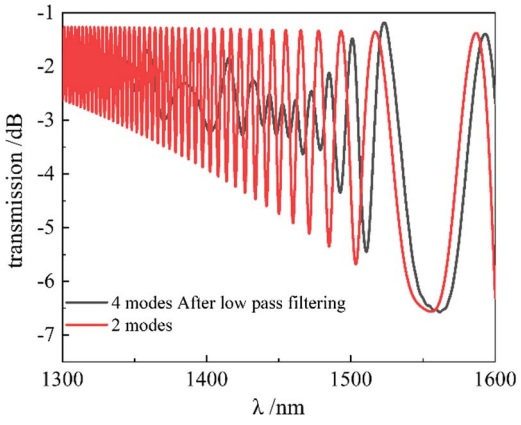

Fig. 6. Transmission spectrum of the first four modes after low-pass filtering and the transmission spectrum of the first two modes.

It can be seen from Fig. 7 that the structure can achieve better linear intensity detection within a certain range of the external RI. For the larger range of other external RI changes, although the wavelength of the depressed peak does not move with the change of the external RI, the linearity of the intensity change is poor. In this regard, the detection of different RI ranges can be achieved by designing different fiber structure parameters.

Through the above-mentioned content, through the analysis of the coupling characteristics of SMF and TCF and the characteristics of long-period grating, a scheme to optimize the MZI of the TCF is proposed. We use a long-period grating in the TCF section of the STS structure to achieve an increase in ER at a specific wavelength, which can reach 62.8 dB and more. In the long-wavelength band, the average ER is greater than in the short wavelength band. Furthermore, when writing a single long-period grating, the structure can produce two sags at short and long wavelengths, and it changes symmetrically as the grating period changes. Different from an intensity detecting

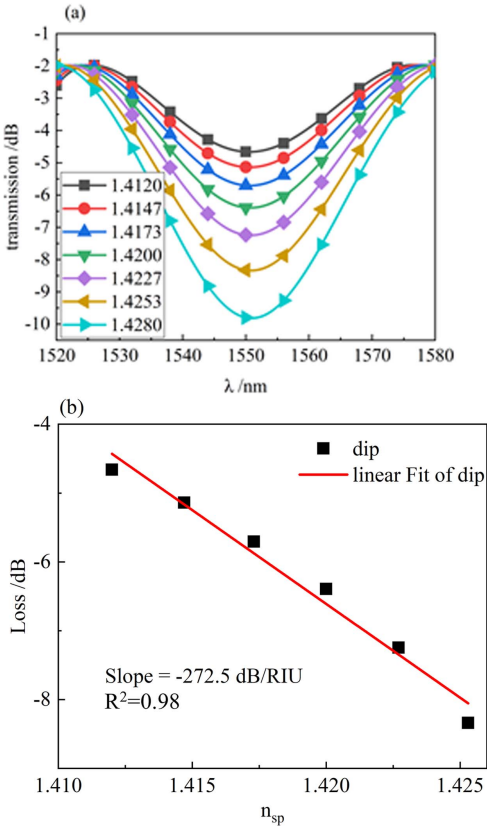

Fig. 7. (a) Variation of the transmission spectrum with external RI. (b) Relationship between light intensity and external RI.

sensor with a long-period grating[21,22], the wavelength of the characteristic peak is fixed at the phase matching point. Intensity detection for different RI ranges can be achieved by changing the structural parameters of the fiber. The sensitivity is −272.5 dB/RIU, and the linearity is good. The special comb spectrum characteristics produced by it can significantly expand the application of TCF.

For different application scenarios, on the basis of keeping the STS structure unchanged, the sensitivity and sensing range can be changed by adjusting the period of the written long-period grating, which reduces manufacturing difficulty and cost. The STS structure has a low insertion loss, and the special double sag feature can be applied to the special device.

In summary, the coupling characteristics of TCF after writing the long-period grating to the SMF were analyzed in detail by simulation, and the influence of different parameters on its ER performance in a certain wavelength range was discussed. The ER can reach 62.8 dB. The structure can provide two high-depth depressions, both in the short wavelength range and the long wavelength range. After optimizing the parameters by simulation, structural parameters can be designed for different target RIs. The sensitivity is −272.5 dB/RIU, and it also has a great linearity. The structure has a low insertion loss, low manufacturing difficulty, and high application space for expansion.

This work was supported by the National Natural Science Foundation of China (Nos. 61827817 and 61525501).

References

1. M. H. Zhou, X. Y. Dong, J. Y. Yang, L. I. Yi, S. Q. Zhang, and S. Z. Jin, J. Optoelectron. Laser **27**, 587 (2016).
2. M. Zhou, X. Dong, and X. Liu, in *International Conference on Optical Communications and Networks* (2017), p. 1.
3. Y. Zhang, Z. Liu, Z. Guo, S. Yuan, D. Feng, X. Dong, and C. Yao, Acta Opt. Sin. **22**, 89 (2002).
4. Y. Zhang, Y. Ren, M. Dong, F. Meng, and L. Zhu, Chin. Opt. Lett. **16**, 120601 (2018).
5. A. M. Vengsarkar, P. J. Lemaire, J. B. Judkins, V. Bhatia, T. Erdogan, and J. E. Sipe, J. Lightwave Technol. **14**, 58 (1996).
6. Y. Wang, C. Fu, C. Liao, and Y. Wang, in *Australian Conference on Optical Fibre Technology* (2016), paper JM6A.31.
7. M. Jiang, Z.-M. Wang, Z.-Z. Zhao, K. Li, and F. Yang, Sensor Rev. **38**, 79 (2018).
8. J. Xing, J. Wen, J. Wang, F. Pang, Z. Chen, Y. Liu, and T. Wang, Chin. Opt. Lett. **16**, 100604 (2018).
9. X. Dong, Z. Xie, Y. Song, K. Yin, D. Chu, and J. A. Duan, Chin. Opt. Lett. **15**, 090602 (2017).
10. Q. Wu, Y. Semenova, P. Wang, and G. Farrell, J. Opt. **13**, 125401 (2011).
11. W. Wang, X. Dong, D. Chu, Y. Hu, X. Sun, and J.-A. Duan, AIP Adv. **8**, 055104 (2018).
12. B. Gu, W. Qi, J. Zheng, S. Ping, and F. Luan, in *Asia Communications and Photonics Conference* (2013), paper AF4H.2.
13. B. Gu, W. Qi, J. Zheng, Y. Zhou, P. P. Shum, and F. Luan, Opt. Lett. **39**, 22 (2014).
14. B. Gu, W. Qi, Y. Zhou, J. Zheng, S. Ping, and F. Luan, in *Optical Fiber Communications Conference and Exhibition* (2014), paper Th2A.34.
15. A. Cusano, A. Iadicicco, P. Pilla, L. Contessa, S. Campopiano, A. Cutolo, and M. Giordano, Opt. Lett. **30**, 2536 (2005).
16. L. C. Bobb, P. M. Shankar, and H. D. Krumboltz, J. Lightwave Technol. **8**, 1084 (1990).
17. Q. Wu, Y. Semenova, P. Wang, and G. Farrell, Opt. Express **19**, 7937 (2011).
18. J. Zheng, L. Pei, T. Ning, J. Li, C. Zhang, S. Ma, and Z. Ruan, Opt. Express **26**, 9182 (2018).
19. Q. Wang and G. Farrell, Opt. Lett. **31**, 317 (2006).
20. Y. Xu, P. Lu, J. Song, L. Chen, X. Bao, and X. Dong, in *IEEE Sensors* (2013), p. 1.
21. R. Falate, O. Frazão, G. Rego, J. L. Fabris, and J. L. Santos, Appl. Opt. **45**, 5066 (2006).
22. H. Sakata and H. Ito, Opt. Commun. **280**, 87 (2007).